Storage and Transport of Charge in Redox Conductive Polymers Probed with Electron Spin Resonance Spectroscopy

Ilia Romanovich Kulikov

Berlin
August 2023

2

Erster Gutachter: Prof. Dr. Jan Behrends
Zweiter Gutachter: Prof. Dr. Kirill Bolotin
Tag der Disputation:

Contents

$\vec{e}_x, \vec{e}_y, \vec{e}_z, t$	Laboratory frame of reference
$\vec{S} = \left(\hat{S}_x, \hat{S}_y, \hat{S}_z \right)$	Spin operator
$h = 6.62607015 \times 10^{-34}$ J $\times$ s	Planck constant
$g_e = -2.00231930436118(27)$	Electron g factor
$\mu_B = 9.2740100783(28) \times 10^{-24}$ J/T	Bohr magneton
$h = 1.25663706212(19) \times 10^{-6}$ N/A^2	Permeability of free space
ϵ	Relative permittivity
$\vec{B_0} = B_0 \vec{e}_z$	Static magnetic field
cwEPR	Continuous wave electron paramagnetic resonance
pEPR	Pulsed electron paramagnetic resonance
EDMR	Electrically detected magnetic resonance
DUT	Device under testing
ORB	Organic radical battery
WE	Working electrode (cathode, "+")
CE	Counter electrode (anode, "-")
RE	Reference electrode
SoC	State of charge
ESOC	EPR-detected SoC
CV	Cyclic voltammogram
GCD	Galvanostatic charge-discharge
TEMPO	2,2,6,6-tetramethylpiperidine-1-oxyl
pDiTBuS	Poly-di-TEMPO-Butyl-Salen
PTMA	Poly-TEMPO-methacrylate
EDFS	Echo-detected field sweep
T_1	Spin-lattice relaxation time
T_m	Phase memory time
t_d	Microwave detector dead time

Table 1: List of abbreviations

Chapter 1

Introduction

Life needs energy to continue its spread. Plants use photosynthesis to separate carbon from oxygen and to grow. Higher life forms as humans consume energy during the day and during the night, being dependent on the available energy source [?]. While fossil fuels are still the major source of energy [?] and while fire is used to convert the Joules that hold together hydrocarbon molecules into a "horse power" of a combustion engine and kilowatt-hours in a power socket, there are cleaner and more efficient ways to harvest energy. Photosynthesis had inspired the creation of solar panels that convert the sunlight into electricity, the atom had been tamed in the core of a nuclear reactor to power cities; we can extract energy from sound [?], wind and waves and from the heat of the planet. Moreover, there are hopes and continuous attempts to achieve nuclear fusion [?] - the creation of an artificial Sun by melting together atomic cores - the virtually inexhaustible and clean source of energy. The oil and gas are limited and unevenly distributed resources, wind does not always blow, the Sun does not shine at night, the wild Nature is still unpredictable and the extracted energy has to be stored in order to level out its production and consumption.

With the rise of the technological era, over the last century, energy has been delivered to our homes in form of electricity. Energy storage systems such as fuel cells, supercapacitors and batteries are crucial elements for powering portable electronics and vehicles, or for balancing a power grid with a renewable energy source. [15]. Two opposite electric charges separated from each other can store energy in an electrostatic field. It is possible to accumulate many charges on the plates of a capacitor and store some energy [?], but due to the technological difficulties, electrochemical cells are commonly used instead. An electrochemical cell is an energy storage device and a power source that undergoes a chemical reaction to transfer the electric charge from one of its components to another through an external circuit. A simple electrochemical cell consists of three elements: two spatially separated materials called electrodes, and a solution of mobile ions between them called electrolyte. The two electrodes have different work functions, or, chemically speaking, reduction-oxidation (redox) potentials. When the electrodes of the cell are connected through an external circuit, the electrons flow through the circuit and the ions in the electrolyte rearrange to maintain charge balance [31]. While the cell delivers the electric current to the circuit, a chemical reaction is happening on its electrodes: the positively charged electrode, called cathode, is being reduced, obtaining electrons from the negatively charged anode through the external circuit. The anode loses electrons and is being oxidized. The speed, reversibility, released by-products and physical conditions of this redox reaction are the key factors that define the performance of an electrochemical cell. This reaction had been of great interest for the field of energy storage, particularly, electrochemistry, where numerous characterization techniques have been developed to optimize the architecture of batteries.

Stable, capacious and powerful batteries have become of great demand for today's energy driven society [49, 48, 35]. The advances in lithium ion technology for rechargeable batteries have enabled energy densities that make it possible to battery-power a wearable Internet-of-things device [24, 28], an

airplane [19] or a house [4, 13]. Still, the application of lithium ion batteries is limited by irreversible processes [23, 8, 53] that occur upon extreme operating conditions such as high power demand [52, 12] or over-discharge [27]. Such degradation processes limit the performance of a battery by lowering its safe operating power, resulting in lower power density and longer charging times. The challenge to overcome these limitations, together with low abundance of Lithium, Cobalt and rare earth metals, [48, 15] and the toxicity of the manufacturing process [37, 36] is motivating research and development of advanced battery technologies [3]. This requires understanding of charge transport and degradation pathways in energy storage materials as well as exploring novel materials such as materials based on organic precursors [26, 20].

Organic radical batteries (ORB) based on redox polymers containing stable radicals [32] have been shown to compete with or even outperform conventional Li based batteries in terms of power densities [43] with the additional benefit of being free from rare precursors, inheriting mechanical properties of plastics and electrical properties of semiconductors [7, 2, 10]. Advanced molecular design techniques allow for tuning of the electrochemical properties of the redox polymers [16], that brings in a rich variety of organic energy storage materials [47, 46, 17] and creates a large room for their optimization.

Redox conductive conjugated polymers containing TEMPO (2,2,6,6-tetramethylpiperidine-1-oxyl) redox groups, as pDiTBuS (poly-di-TEMPO-Butyl-Salen) shown in Figure 3.1, demonstrate particularly promising energy and power densities [45]. The pDiTBuS was designed as a cathode material: it is oxidized when the electrochemical cell containing this material is charged. A film of pDiTBuS comprises a high concentration of redox active stable nitroxyl radicals attached to a conjugated polymer backbone that interconnects them as a molecular wire. Such system may be viewed as a highly disordered molecular hole-transporting semiconductor (the poly-NiSalen backbone) that contains a large amount of hole traps (TEMPO groups) attached to it with butyl linkers. When the film is reduced (discharged), the TEMPO groups are in the radical state and act as unfilled traps. Upon oxidation (charging), the TEMPO fragments lose an unpaired electron and acquire a positive charge, so the traps are being filled with holes.
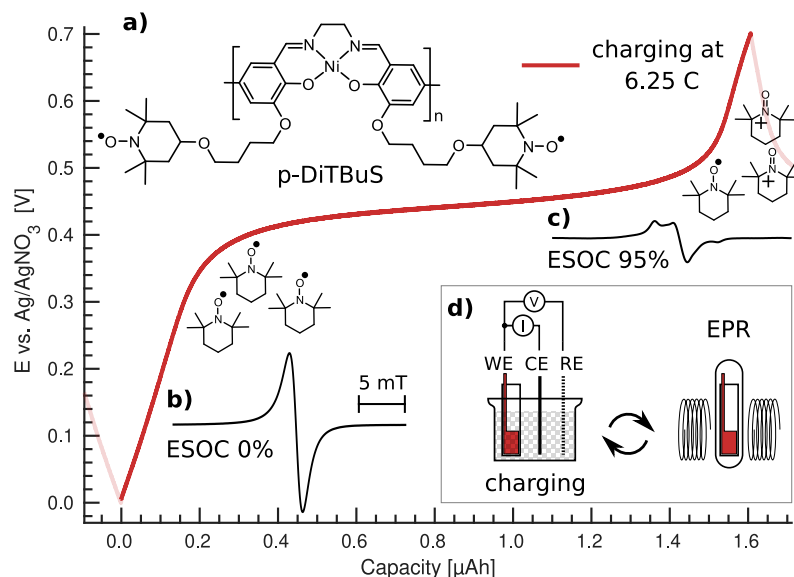
Figure 1.1: Galvanostatic charge-discharge curve for a pDiTBuS cathode film at 10 μA (6.25 C), chemical structure of pDiTBuS (a), normalized cwEPR spectral signatures for reduced (b) and oxidized (c) states. Scheme of the ex-situ EPR measurement on the pDiTBuS half cell (d).

The flexible molecular design together with questions regarding unresolved charge transport- and performance limiting mechanisms have inspired a variety of characterization techniques to be developed and applied to both energy storage materials and energy storage devices, operando and ex-situ. Together

with electrochemical characterization as the standard method for studying the properties of energy storage materials[43, 51], operando optical microscopy [30], neutron imaging [27] and X-ray diffraction [38] were applied to monitor irreversible structural deformations during extreme charging of Li cells.

UV and IR spectroscopy turned out to be particularly useful for studying organic energy-storage materials. For instance, it was possible to observe formation of positive polarons in the NiSalen backbone of the pDiTBuS upon its oxidation [5]. Since the electrochemical processes happen within the bulk of the energy storage material and involve changes in the spin states, imaging techniques based on magnetic resonance can be applied to obtain structural information on the battery electrodes on the molecular level [34, 29, 25, 1]. NMR was used to study dendrite formation, electrolyte dynamics and intercalation of Li ions[22, 11] in Li cells, including operando imaging [42].

Operando continuous-wave EPR (cwEPR) was applied to study redox kinetics of inorganic battery cathodes [33], radical formation and spin densities in redox polymers [5] and in organic electrochemical cells [14, 21].

Pulsed EPR (pEPR) provides an even more powerful toolbox for material studies with the electron spin as a microscopic structural probe. In particular, pEPR provides access to the dipolar coupling between neighboring electron spins and thus the possibility to determine distances between adjacent redox-active centers using dipolar spectroscopy [39] as in spin-labelled proteins [18, 44]. In addition, the hyperfine coupling between electron and nuclear spins in close vicinity can be measured by electron spin echo envelope modulation (ESEEM) and electron nuclear double resonance (ENDOR) techniques and can thus elucidate the degree of delocalization for charge carriers in ORB materials in a similar way as in organic seminconductors [6].

EDMR is allowing to manipulate the spin of an electron that tunnels through a disordered media such as the amorphous silicon in a solar cell, through intertwined fragments of conjugated polymers in an organic solar cell or an organic field-effect transistor.

Chapter 2

Electrochemical Energy Storage in Redox Conductive Polymers

Batteries based on conjugated polymers containing stable radical moieties as high-capacitance groups represent a promising class of future electrochemical power sources.[32, **?**, **?**, **?**] They combine the advantages of high-power supercapacitors, namely high discharge rates, and the high energy density of conventional lithium-ion technology. A further beneficial property of organic materials over traditional inorganic materials is their availability and the low cost of the starting materials for the synthesis of the target polymers in conjunction with good mechanical properties.[15, 31, 7]

While active electrode materials with nitroxide radicals as redox-active groups are ideally suited for organic radical batteries (ORBs) that exhibit high power densities, the broad application of most nitroxide-based materials is limited by their moderate electrical properties. A promising route towards overcoming the conductivity problem is the use of polymers that combine radical-containing moieties and a conductive backbone. This strategy was successfully followed in a number of studies focusing on different polymers.[**?**, **?**, **?**, **?**, **?**, **?**]

Chapter 3

Operando EPR Spectroscopy of TEMPO-Salen Cathode Films

3.1 Electron Paramagnetic Resonance

3.1.1 The Spin Hamiltonian

Electron Spin   The electron bears an internal angular momentum that is called spin. Spin combines with the charge of the electron to endow the electron with a magnetic moment. The magnetic moment of the electron is quantized: $\mu_e = \mu_B g S$ [9], where S is the spin quantum number, the eigenvalue of the spin operator $\vec{S}$, that equals $S = 1/2$ for an electron. When an electron is placed in a static magnetic field $\vec{B_0} = B_0 \vec{e_z}$, its magnetic moment precesses about the field direction with the Larmor frequency $\omega_L = \gamma B_0$, where $\gamma = \frac{g_e \mu_B}{\hbar} = 28.025$ GHz/T is the gyromagnetic ratio of the electron and g_e is the electron g factor. The projection of the electron's magnetic moment on the direction of the magnetic field can take only discrete values between $-S = -1/2$ and $S = 1/2$, so that the eigenvalues of the z component of the spin operator are also discrete: $\hat{S}_Z|\uparrow\rangle = +\frac{\hbar}{2}|\uparrow\rangle$, $\hat{S}_Z|\downarrow\rangle = -\frac{\hbar}{2}|\downarrow\rangle$. The two eigenfunctions of $\hat{S}_Z$ are called the spin-up state $|\uparrow\rangle$ and the spin-down state $|\downarrow\rangle$. The two corresponding eigenvalues $\pm\frac{\hbar}{2}$ define the energy difference between the states $|\uparrow\rangle$ and $|\downarrow\rangle$, that is known as the Zeeman splitting.

Zeeman Splitting   The energy of an unpaired electron placed in the external magnetic field $\vec{B_0}$ is the eigenvalue of the spin Zeeman Hamiltonian: $\hat{H}_{EZ} = \mu_B g \vec{B_0} \cdot \vec{S}$. In the laboratory frame of reference $\vec{B_0} \parallel \vec{e_z}$, $\left[\hat{H}_{EZ}, \hat{S}_z\right] = 0$, so $\hat{H}_{EZ}$ and $\hat{S}_Z$ share the two eigenfunctions $|\uparrow\rangle$ and $|\downarrow\rangle$. The Zeeman energies of the electron are $E_{EZ}^{\pm} = \pm\frac{\hbar}{2}\mu_B g B_0$.

Nuclear Spin and Nuclear Zeeman Splitting   A proton also bears an internal angular momentum $S = 1/2$ that results in a magnetic moment $\mu_p = \mu_e \frac{m_e}{m_p}$, that is $\frac{m_e}{m_p} \approx 1836$ times smaller than the electron's magnetic moment. A neutron bears no charge but still has an internal angular momentum $S = 1/2$. An atomic nucleus that consists of protons and neutrons can have a magnetic moment, depending on the mutual orientations of their spins and on the nuclear charge. A nitrogen nucleus has 7 protons and 7 neutrons that total in a nuclear spin $I = 1$ which, with the g factor for the nitrogen nucleus g_N, results in the nuclear magnetic moment of $\mu_N = \mu_B g_N \frac{m_e}{m_N} I$ that splits into three Zeeman energy levels corresponding to $I = -1, 0, +1$, analogously to the electron with $S = 1/2$. The nuclear Zeeman splitting is more than three orders of magnitude weaker than the electron Zeeman splitting because of the difference in the masses of the particles.

Hyperfine Interaction   The magnetic moments of an electron and a magnetic nucleus, such as nitrogen, couple in the hyperfine interaction [40]: $H_{HF} = \vec{S} \mathbf{A} \vec{I} = H_F + H_{DD}$ with the hyperfine tensor $\mathbf{A}$. The

13

isotropic part $H_F = a_{iso}\vec{S}\vec{I}$, or the Fermi contact interaction, scales with the probability density of the electron at the position of the nucleus $a_{iso} = \frac{2}{3}\frac{\mu_0}{\hbar}g_e\beta_e g_n\beta_n|\psi(0)|^2$. The anisotropic part $H_{DD} = \vec{S}\mathbf{T}\vec{I}$ with the dipolar coupling tensor $\mathbf{T}$ takes into account the anisotropic dipole-dipole coupling between the magnetic moments of the electron and the nucleus.

Nuclear Quadrupole Moment The nitrogen nucleus has a spin greater than 1/2 which alters the charge distribution within the nucleus which gives rise to a non-vanishing nuclear electrical quadrupole moment Q. The interaction between the asymmetrically distributed charge and the gradient of the electric field at the nucleus is given by the nuclear quadrupole Hamiltonian $H_{NQ} = \vec{I}\mathbf{P}\vec{I}$ with the nuclear quadrupole tensor $\mathbf{P}$ that describes the coupling of the nuclear quadrupole moment to the electric field gradient.

Exchange Interaction In a system of closely placed electrons, such as in a film of densely packed nitroxide radicals, the electron orbitals may overlap significantly and the radicals may exchange electrons. The energy required to exchange the electrons is called the Heisenberg exchange coupling $H_{exch} = \vec{S}_1\mathbf{J}\vec{S}_2$, that becomes considerably large at inter-spin distances below $r < 1.5$ nm or with a large spin delocalization [41]. The positive $\mathbf{J}$ corresponds to a weak coupling between S_1 and S_2 which leads to an antiferromagnetic or antiparallel alignment of spins with a total $S = 0$, whereas the negative $\mathbf{J}$ causes the strong inter-spin coupling which leads to a ferromagnetic alignment with $S = 1$.

Magnetic Dipole-Dipole Interaction The dipole-dipole interaction between the two neighboring electron spins contributes one more term to the spin Hamiltonian: $H_{dd} = \vec{S}_1\mathbf{D}\vec{S}_2$ that depends on the distance between the spins.

3.1.2 Instrumentation

EPR Hardware First observed in 1944 [50], the phenomenon of electron paramagnetic resonance had become a tool for probing local molecular environments in species that contain an unpaired electron. A free electron, that does not interact with its environment and has $g = g_e$, experiences a Zeeman splitting of $\Delta E = g\mu_B B_0$, that corresponds to the energy of a photon with a frequency of $\nu = \Delta E/h$. At $B_0 \approx 0.3$ T, a microwave photon with $\nu \approx 9.5$ GHz can drive the magnetic dipole transition between $|\uparrow\rangle$ and $|\downarrow\rangle$, that is called the spin flip. The microwave sources are historically[**?**] available in a number of discrete bands, one of them is known as *X* band for the range between 8 and 12 GHz. To ensure that only the magnetic component of the microwave photon is interacting with the sample, a resonating cavity is used, where a standing microwave is formed, so that in the center of the cavity, the magnetic component of the microwave is maximized and the electric component is quenched. The sample is inserted in the center of the cavity and the external magnetic field is swept. When the resonance condition is met **??**, the spin flip occurs and the photon is being absorbed by the sample. The resonance absorption of microwaves can be detected by a small decrease in the quality factor Q of the resonating cavity, as the magnetic field is being scanned and the microwave frequency is kept constant. The change in the Q factor during the spin flip leads to temporal decoupling of the resonator, that causes reflections of the microwave that would have entered the resonator off resonance. The intensity of the microwaves is measured with a biased semiconductor diode that has a linearly changing conductivity in the range corresponding to the incident microwave power. A phase sensitive detection with the shallow modulation of B_0 increases the signal-to-noise ratio (SNR), and yields the derivative of the resonance absorption profile. The typically high $Q \gg 1$ factor of the resonating cavity further increases the SNR.

3.2 EPR Spectroscopy of a Charging Electrochemical Cell

There is a number of difficulties when it comes to an EPR experiment on a working electrochemical cell. The cell must contain mobile ions between its electrodes. The ions are normally produced as products of dissociating salts. To overcome break the salt into the ions (a cation and an anion), a solvent with large

dipole moment is needed. Solvents with large dipole moments, as acetonitrile (CH_3CN, $\epsilon \approx 37.5$) or water ($\epsilon \approx 78.4$), have large dielectric constants which results in a non-resonant absorption of microwaves. Therefore, the cell containing liquid electrolyte absorbs microwaves and lowers the sensitivity of the EPR experiment. Furthermore, due to a finite dimension of cell, not only the magnetic component of the microwave is interacting with the electrolyte, but also the electric one - this results in heating of the electrolyte in a similar fashion as in a microwave oven. The heating of the electrolyte leads to a faster degradation of the cell and does not allow for long systematic measurements.

Another general issue with the operando EPR and EDMR experiments is that the device under testing (DUT) has to have metal electrodes that deliver current to it. Metals, placed in a microwave cavity, change the distribution of the electromagnetic field in it - that weakens the magnetic component at the device and at the same time strengthens the electric component. It is the magnetic dipole transition that is causing the magnetic resonance, so the weakening of the magnetic component by introducing the metal electrodes further decreases the magnetic resonance response. The increased electric component causes heating to temperatures that can be critical for the DUT operation.

3.2.1 Fabrication of EPR-compatible Electrochemical Cells

3.2.2 EPR Spectra During a Charge-Discharge Cycle

3.2.3 Spectral Simulations

3.2.4 Quantitative Analysis of Potential-Dependent EPR Spectra

3.2.5 EPR-Detected State Of Charge

3.2.6 Formation of Singlet Spin States in a Reduced Cathode Film

3.2.7 Monitoring of Degradation Processes

3.2.8 Monitoring of Self Discharge

3.2.9 Electrochemical Cells with Solid Electrolyte
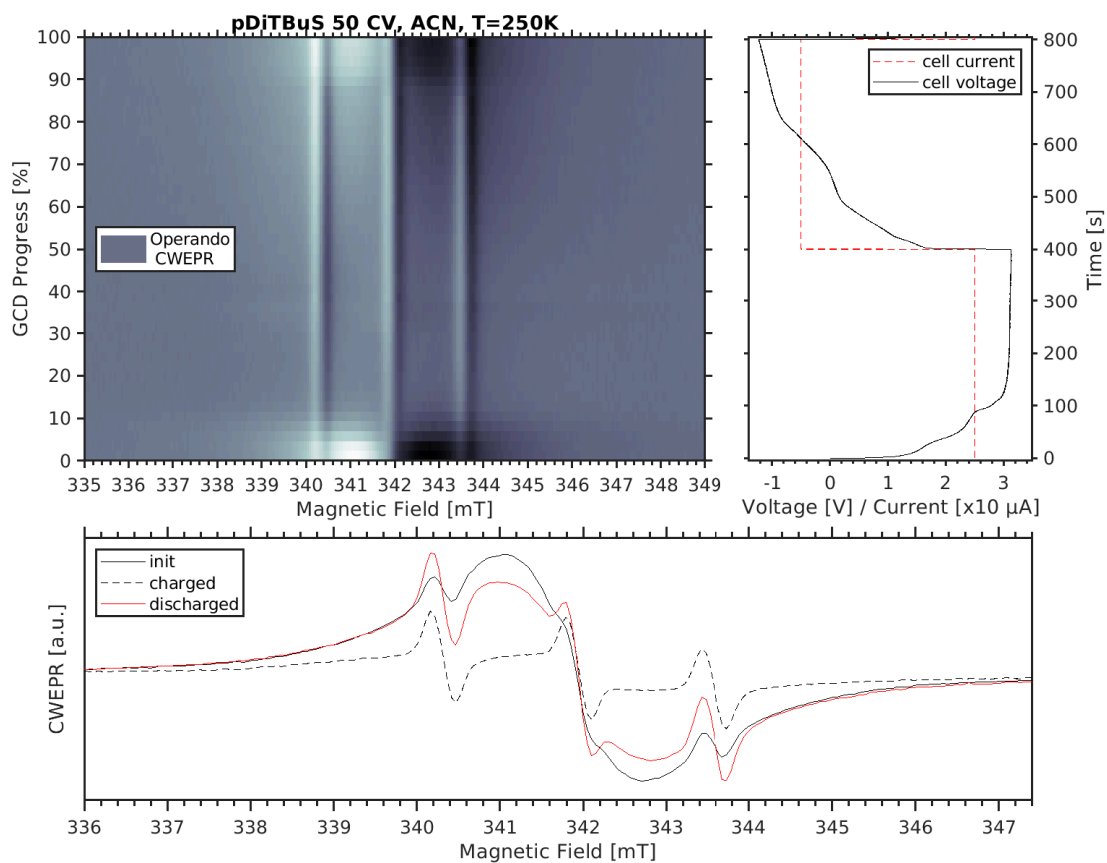
3.2.10 Low Temperature Measurements

Figure 3.1: XXX

Chapter 4

Pulsed Electron Paramagnetic Resonance Spectroscopy of Densely Packed Nitroxide Radicals

4.1 Coherent Spin Motion under Pulsed Microwave Field

When a spin system is excited with a microwave pulse, its evolution is described with the set of equations that is known as the Bloch equations.

4.1.1 Bloch Equations

4.1.2 Spin Relaxation Times

4.1.3 Spin Packets

4.2 Instrumentation

4.2.1 Pulse Sequences and Measurement Techniques

The Refocused Spin Echo

The Hahn Echo sequence consists of two pulses, the $\pi/2$ pulse and the π pulse, separated in time by τ: $\pi/2 - \tau - \pi - \tau - echo$. Initially, the macroscopic magnetization of the spin system is aligned along $\vec{B_0}$: $\vec{M_0} = M_Z \, \vec{e_Z}$. The $\pi/2$ microwave pulse has such length $t_{\pi/2}$ and amplitude B_1 that, during the pulse, $\vec{M}$ nutates to the xy plane, where it keeps precessing about $\vec{e_Z}$ after the end of the pulse. The difference in local environments for each individual spins in the spin packet, as well as the interactions between the spins, that make up $\vec{M}$, leads to slightly different precession frequencies ω_L^i of the spins. After some time τ, the difference in the precession frequencies translates into the differences in phases so that the vector sum of the excited spins averages down to $\vec{0}$ for sufficiently long τ. In other words, the excited spin packet dephases with time. The dephasing due to different local spin environments can be reversible if the deviations of the precession frequencies do not depend on time, as is the case for separated electrons in an inhomogeneous solid. In such case, a π pulse can be applied to the spin system to flip every single spin in the dephased spin packet by 180deg in a plane containing $\vec{e_Z}$, so that the spins keep precessing in the xy plane, but the direction of precession is inverted for them, leading to the effect that is opposite to the initial dephasing. So a τ after the π pulse excites the spin packet, the accumulated phase differences become the smallest and the packet recovers its macroscopic magnetization $\vec{M}$ that oscillates in the xy plane with $\langle \omega_L^i \rangle$ and can be detected. The recovered $\vec{M}$ at $t = \tau$ after the π pulse is called the refocused spin echo. The difference in ω_L^i

leads to a further dephasing of the considered spin packet and to the vanishing of $\vec{M}$.

Spin Echo Decay and Phase Memory Time

Inversion Recovery and Spin-Lattice Relaxation Time

4.2.2 Broad-Band Excitation and Instantaneous Diffusion

4.3 Pulsed EPR Spectroscopy of a charged pDiTBuS Cathode film
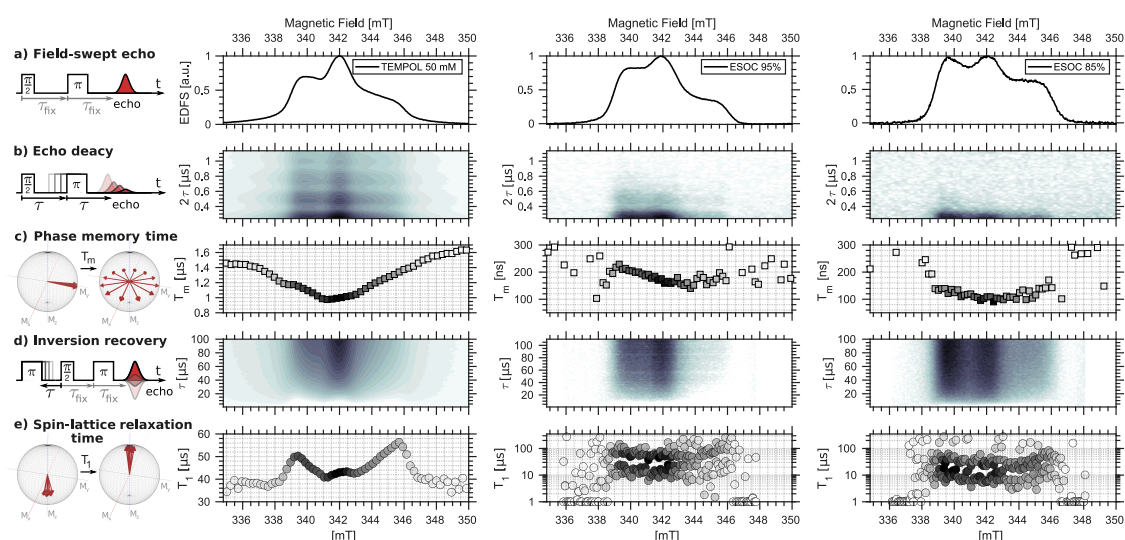
4.3.1 Field Swept Echo of a charged pDiTBuS Cathode film

Figure 4.1: XXX

4.3.2 Estimation of Local Spin Concentrations with Instantaneous Diffusion

4.3.3 Spin Relaxation in a charged pDiTBuS Cathode Film

4.3.4 Pade-Laplace Deconvolution of Echo Decay Transients

4.3.5 Detection of Domains with Poor Conductivity

4.3.6 Towards Imaging of Spin Concentration in Battery Electrodes

Chapter 5

Longitudinally Detected Electron Paramagnetic Resonance in Systems with Short Relaxation Times

LOD lets us look behind the protection pulse.

Chapter 6

Electrically Detected Magnetic Resonance on a Cathode of an Organic Radical Battery

With EDMR we observe the hopping charge as it travels to the charge bearing group through the electrode.

6.0.1 Spin Blockade and Spin-Dependent Recombination

6.0.2 Instrumentation

6.0.3 Device Fabrication

1N4007 Si diode

A commercial 1N4007 p-n Si diode was modified to use as a standard for the EDMR experiments. The plastic housing of the diode was opened and the copper leads were etched out to reduce the metal content of the sample that strongly suppresses the B_1 field needed for reaching the resonance condition, and, additionally, leads to the heating of the sample which affects the current through the diode. The diode with the opened housing was placed into a droplet of concentrated nitric acid (65% HNO_3) and the etching process was observed in a microscope. When the copper leads have reduced in size so that only a thin layer of copper was covering the Si crystal, the etching reaction was stopped with ethanol. Two $\oslash$ 0.1 mm Ag wires were used to connect the diode to the detection circuit through the screened coaxial cables. The device was placed in a $\oslash$ 4.9 mm OD quartz EPR sample tube.

DPP-DTT Organic Ambipolar Field Effect Transistor

An organic field-effect transistor was fabricated by Z. Wang in the Cavendish Laboratory of the University of Cambridge in a glovebox filled with Ar. A 3.5 mm wide, 1 mm thick quartz substrate was carrying two on-substrate meander-shaped Au electrodes as the drain and the source electrodes. A thin film of DPP-DTT was spin-coated on the on-substrate electrodes. A layer of ???? was spin-coated as the gate isolator on top of the DPP-DTT film. The Au gate electrode was evaporated onto the isolator layer through a shadow mask. The metal electrodes were extended with a wire bonder, and soldered to thick Cu wires. The device was encapsulated in a $\oslash$ 4.9 mm OD quartz EPR sample tube.

339 **pDiTBuS Organic Radical Battery**

6.0.4 EDMR signal in a 1N4007 Si Diode
340

6.0.5 EDMR signal in an Organic Field Effect Transistor
341

6.0.6 EDMR signal in a TEMPO-Salen Electrochemical Cell
342

6.0.7 Distribution of Current Density in On-Substrate Meander-Shaped Electrodes
343

344 Meander-shaped electrodes shown in Figure 6.1 are used to study properties of thin conductive films. The
345 distribution of electric potential and the current within a film of poor conductivity and a finite thickness be
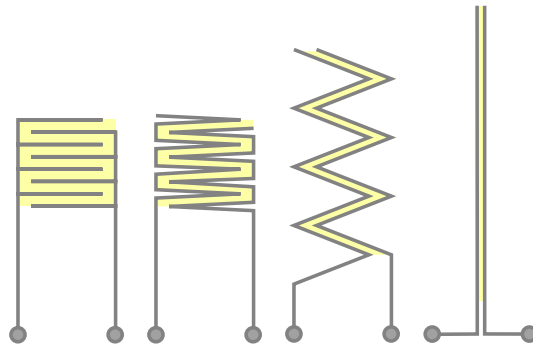346 not obvious.

Figure 6.1: Transformation of the meander-shaped electrode grid into two linear electrodes

347 A numerical solution was found to the distribution of the current density $\vec{j}$ within a film of a finite
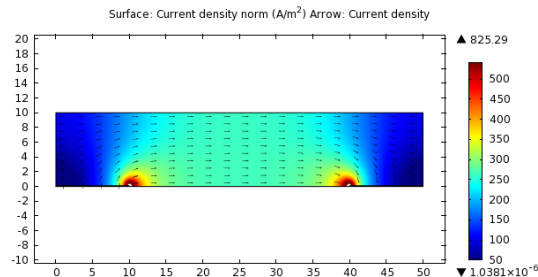348 thickness, connected by two metal electrodes. Two cases were considered, a thick film and a thin film.

Figure 6.2: Distribution of electric current in a thick polymer film. The current is uniform in the middle of
the film. Let us see, whether we can apply the simple, bulk formula to this structure.
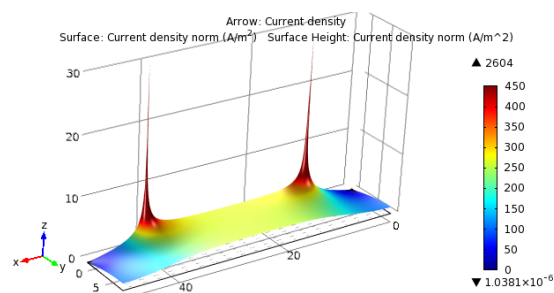
Figure 6.3: Thick film. The current is uniform in the middle of the film. It is better seen on this 3d plot. Let us see, whether we can apply the simple, bulk formula to this structure. I think we do not gain a lot of error by saying that the current is uniform within the whole film.
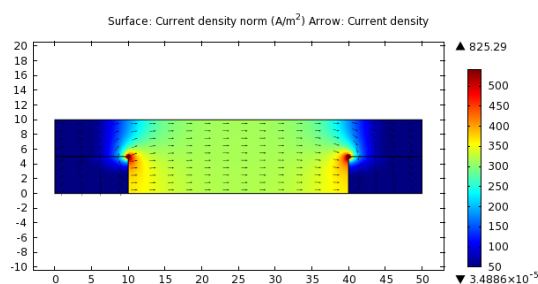

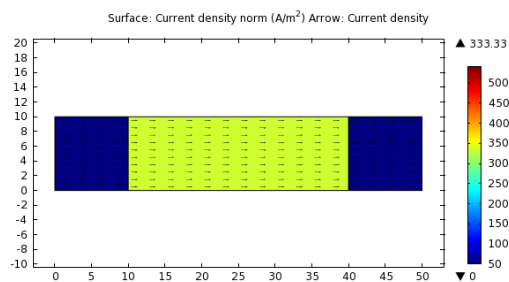Figure 6.4: Distribution of electric current in an intermediate polymer film

Figure 6.5: Distribution of electric current in a thin polymer film
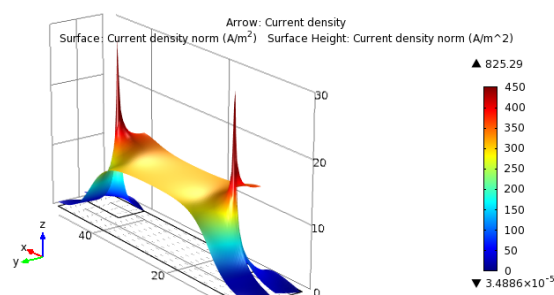

Figure 6.6: Very high values of the computed distribution of the current density in a film of intermediate thickness due to the sharp edges of the contacts.

Chapter 7

The Deep-Trap Model of a TEMPO-Salen Electrode Film

A TEMPO-Salen redox conductive film can be seen as a p-type molecular semiconductor enriched with hole traps. The conductive Salen backbone is carrying positive polarons and bipolarons that delocalize within the polymer fragments and effectively hop between them. When a polaron, traveling through the Salen backbone, approaches a charge-bearing TEMPO$^\bullet$ fragment, it rather hops to it, recombining with the unpaired electron of the radical. The TEMPO$^\bullet$ oxidizes and becomes TEMPO$^+$ which now bears a positive charge. Therefore, TEMPO$^\bullet$ is a trap for the positive charge carrier (hole) that is injected into the poly-Salen network.

The charging of a TEMPO-Salen cathode film can be seen as a consequent filling of traps in a hole-transporting semiconductor. The relative orientations of the spins of the recombining particles defines the probability of the recombination process. At low SoC, the hole, traveling through the polymer, has many TEMPO$^\bullet$ candidates to recombine with. Some of the TEMPO$^\bullet$ radicals are in the $|\uparrow\rangle$ state, some are in the $|\downarrow\rangle$ state, - so the recombination process does not depend on the spin state of the hole, as it can recombine to the radical in the "appropriate" spin state. At higher SoC, the more TEMPO$^\bullet$ become occupied with holes and become TEMPO$^+$, the longer distance the hole needs to overcome to meet the TEMPO$^\bullet$ that has the "appropriate" spin state. In this case, the recombination process must become spin dependent and an EDMR signal appears.

no edmr data to prove that, yet. The short distance between the TEMPO$^\bullet$ in the TEMPO-Salen film leads to the strong exchange interaction between the neighboring TEMPO$^\bullet$. That leads to the anti-parallel alignment of their spins and makes them EPR silent and causes a drastic difference between the Coulomb counting and the ESOC data. The formation of bipolarons in the Salen backbone and the close packing of TEMPO$^\bullet$ may lead to the two-hole-two-electron recombination that can explain the high charging rates of TEMPO-Salen films.

Chapter 8

Conclusions and Outlook

What hasnt worked so far is the EDMR. It would be super cool to see the signal, but my devices don't live that long. LOD also did not work up to now. Adjusting the pulse train rate to the eigenfrequency of the ENDOR coils turned out to be an irresistible obstacle.

Bibliography

[1] Robert Bittl and Stefan Weber. Transient radical pairs studied by time-resolved epr. *Biochimica et Biophysica Acta - Bioenergetics*, 1707:117–126, 2005.

[2] Nerea Casado and David Mecerreyes. Chapter 1: Introduction to redox polymers: Classification, characterization methods and main applications, 2021.

[3] Florian Degen and Marius Schütte. Life cycle assessment of the energy consumption and ghg emissions of state-of-the-art automotive battery cell production. *Journal of Cleaner Production*, 330:129798, 2022.

[4] Boucar Diouf and Christophe Avis. The potential of li-ion batteries in ecowas solar home systems. *Journal of Energy Storage*, 22:295–301, 2019.

[5] Evgenia Dmitrieva, Marco Rosenkranz, Julia S. Danilova, Evgenia A. Smirnova, Mikhail P. Karushev, Irina A. Chepurnaya, and Aleksander M. Timonov. Radical formation in polymeric nickel complexes with n2o2 schiff base ligands: An in situ esr and uv–vis–nir spectroelectrochemical study. *Electrochimica Acta*, 283:1742–1752, 2018.

[6] M. Fehr, J. Behrends, S. Haas, B. Rech, K. Lips, and A. Schnegg. Electrical detection of electron-spin-echo envelope modulations in thin-film silicon solar cells. *Physical Review B - Condensed Matter and Materials Physics*, 84:1–5, 11 2011.

[7] C Friebe and U S Schubert. High-power-density organic radical batteries. *Topics in Current Chemistry*, 375:1–35, 2017.

[8] Yangyang Fu, Song Lu, Kaiyuan Li, Changchen Liu, Xudong Cheng, and Heping Zhang. An experimental study on burning behaviors of 18650 lithium ion batteries using a cone calorimeter. *Journal of Power Sources*, 273:216–222, 1 2015.

[9] Walther Gerlach and Otto Stern. Der experimentelle nachweis der richtungsquantelung im magnetfeld. *Zeitschrift für Physik*, 9:348–352, 1922.

[10] Nicolas Goujon, Nerea Casado, Nagaraj Patil, Rebeca Marcilla, and David Mecerreyes. Organic batteries based on just redox polymers: Abstract. *Progress in Polymer Science*, 122:101449, 2021.

[11] Cristina Grosu, Chiara Panosetti, Steffen Merz, Peter Jakes, Stefan Seidlmayer, Sebastian Matera, Rüdiger a Eichel, Josef Granwehr, and Christoph Scheurer. Revisiting the storage capacity limit of graphite battery anodes : Spontaneous lithium overintercalation at ambient pressure. *PRX Energy*, 2:1–14, 2023.

[12] Ting Guan, Shun Sun, Fengbin Yu, Yunzhi Gao, Peng Fan, Pengjian Zuo, Chunyu Du, and Geping Yin. The degradation of licoo2/graphite batteries at different rates. *Electrochimica Acta*, 279:204–212, 2018.

[13] Takuma Hirasawa, Mika Yoshida, and Shin'ya Obara. Battery control for leveling the amount of electricity purchase in smart-energy houses. *International Journal of Energy Research*, 45:807–823, 2021.

29

[14] Q Huang, E D Walter, L Cosimbescu, D Choi, and J P Lemmon. In situ electrochemical-electron spin resonance investigations of multi-electron redox reaction for organic radical cathodes. *Journal of Power Sources*, 306:812–816, 2016.

[15] T Janoschka, M D Hager, and U S Schubert. Powering up the future: Radical polymers for battery applications. *Adv. Mater.*, 24:6397–6409, 2012.

[16] Tobias Janoschka, Christian Friebe, Martin D. Hager, Norbert Martin, and Ulrich S. Schubert. An approach toward replacing vanadium: A single organic molecule for the anode and cathode of an aqueous redox-flow battery. *ChemistryOpen*, 6:216–220, 2017.

[17] Tobias Janoschka, Christian Friebe, Martin D. Hager, Norbert Martin, and Ulrich S. Schubert. An approach toward replacing vanadium: A single organic molecule for the anode and cathode of an aqueous redox-flow battery. *ChemistryOpen*, 6:216–220, 2017.

[18] G Jeschke. Deer distance measurements on proteins. *Annual Review of Physical Chemistry, Vol 63*, 63:419–446, 2012.

[19] Josef Kadlec, Radoslav Cipin, Dalibor Cervinka, Pavel Vorel, and Bohumil Klima. Li-ion accumulators for propulsion system of electric airplane vut 051 ray. *Journal of Solid State Electrochemistry*, 18:2307–2313, 2014.

[20] Jihyeon Kim, Youngsu Kim, Jaekyun Yoo, Giyun Kwon, Youngmin Ko, and Kisuk Kang. Organic batteries for a greener rechargeable world. *Nature Reviews Materials*, 8:54–70, 2023.

[21] Ilia Kulikov, Naitik A. Panjwani, Anatoliy A. Vereshchagin, Domenik Spallek, Daniil A. Lukianov, Elena V. Alekseeva, Oleg V. Levin, and Jan Behrends. Spins at work: probing charging and discharging of organic radical batteries by electron paramagnetic resonance spectroscopy. *Energy and Environmental Science*, 15:3275–3290, 2022.

[22] T. Kushida and J. C. Murphy. Volume depencence of the knight shift in lithium. *Physical Review B*, 21:4247–4250, 1980.

[23] Fredrik Larsson, Petra Andersson, Per Blomqvist, and Bengt Erik Mellander. Toxic fluoride gas emissions from lithium-ion battery fires. *Scientific Reports*, 7:1–13, 12 2017.

[24] Yong Hee Lee, Joo Seong Kim, Jonghyeon Noh, Inhwa Lee, Hyeong Jun Kim, Sunghun Choi, Jeongmin Seo, Seokwoo Jeon, Taek Soo Kim, Jung Yong Lee, and Jang Wook Choi. Wearable textile battery rechargeable by solar energy. *Nano Letters*, 13:5753–5761, 2013.

[25] Chao Li, Ming Shen, and Bingwen Hu. Solid-state nmr and epr methods for metal ion battery research. *Wuli Huaxue Xuebao/ Acta Physico - Chimica Sinica*, 36:1–16, 2019.

[26] Yong Lu and Jun Chen. Prospects of organic electrode materials for practical lithium batteries. *Nature Reviews Chemistry*, 4:127–142, 2020.

[27] Tianyi Ma, Siyuan Wu, Fang Wang, Joseph Lacap, Chunjing Lin, Shiqiang Liu, Mohan Wei, Weijian Hao, Yunshi Wang, and Jae Wan Park. Degradation mechanism study and safety hazard analysis of overdischarge on commercialized lithium-ion batteries. *ACS Applied Materials and Interfaces*, 12:56086–56094, 2020.

[28] Praveen Kumar Reddy Maddikunta, Gautam Srivastava, Thippa Reddy Gadekallu, Natarajan Deepa, and Prabadevi Boopathy. Predictive model for battery life in iot networks. *IET Intelligent Transport Systems*, 14:1388–1395, 2020.

[29] Christoph Meier, Jan Behrends, Christian Teutloff, Oleksandr Astakhov, Alexander Schnegg, Klaus Lips, and Robert Bittl. Multi-frequency edmr applied to microcrystalline thin-film silicon solar cells. *Journal of Magnetic Resonance*, 234:1–9, 2013.

[30] Alice J. Merryweather, Quentin Jacquet, Steffen P. Emge, Christoph Schnedermann, Akshay Rao, and Clare P. Grey. Operando monitoring of single-particle kinetic state-of-charge heterogeneities and cracking in high-rate li-ion anodes. *Nature Materials*, 21:1306–1313, 2022.

[31] S Muench, A Wild, C Friebe, B Haupler, T Janoschka, and U S Schubert. Polymer-based organic batteries. *Chemical Reviews*, 116:9438–9484, 2016.

[32] K Nakahara, S Iwasa, M Satoh, Y Morioka, J Iriyama, M Suguro, and E Hasegawa. Rechargeable batteries with organic radical cathodes. *Chem. Phys. Lett.*, 359:351–354, 2002.

[33] Arvid Niemöller, Peter Jakes, Rüdiger A. Eichel, and Josef Granwehr. In operando epr investigation of redox mechanisms in licoo2. *Chemical Physics Letters*, 716:231–236, 2019.

[34] Arvid Niemöller, Peter Jakes, Svitlana Eurich, Anja Paulus, Hans Kungl, Rüdiger A. Eichel, and Josef Granwehr. Monitoring local redox processes in lini0.5mn1.5o4 battery cathode material by in operando epr spectroscopy. *Journal of Chemical Physics*, 148:1–10, 2018.

[35] Naoki Nitta, Feixiang Wu, Jung Tae Lee, and Gleb Yushin. Li-ion battery materials: Present and future. *Materials Today*, 18:252–264, 2015.

[36] Jens F. Peters, Manuel Baumann, Benedikt Zimmermann, Jessica Braun, and Marcel Weil. The environmental impact of li-ion batteries and the role of key parameters – a review. *Renewable and Sustainable Energy Reviews*, 67:491–506, 2017.

[37] Anna Pražanová, Vaclav Knap, and Daniel Ioan Stroe. Literature review, recycling of lithium-ion batteries from electric vehicles, part i: Recycling technology. *Energies*, 15:1–29, 2022.

[38] Kevin J. Rhodes, Roberta Meisner, Melanie Kirkham, Nancy Dudney, and Claus Daniel. In situ xrd of thin film tin electrodes for lithium ion batteries. *Journal of The Electrochemical Society*, 159:A294–A299, 2012.

[39] K. M. Salikhov, S. A. Dzuba, and A. M. Raitsimring. The theory of electron spin-echo signal decay resulting from dipole-dipole interactions between paramagnetic centers in solids. *Journal of Magnetic Resonance*, 42:255–276, 1981.

[40] A Schweiger and G Jeschke. *Principles of Pulse Electron Paramagnetic Resonance*. Oxford University Press, 2001.

[41] A Schweiger and G Jeschke. *Principles of Pulse Electron Paramagnetic Resonance*. Oxford University Press, 2001.

[42] Yongchao Shi and Mingxue Tang. Nmr/epr investigation of rechargeable batteries. *Wuli Huaxue Xuebao/ Acta Physico - Chimica Sinica*, 36:1–13, 2019.

[43] Hiroyuki Takeo Nishide and Suga. Organic radical battery. *Journal of the Society of Mechanical Engineers*, 110:194–195, 2007.

[44] Yu. V. Toropov, S. A. Dzuba, Yu. D. Tsvetkov, V Monaco, F Formaggio, M Crisma, C Toniolo, and J. Raap. Molecular dynamics and spatial distribution of toac spin-labelled peptaibols studied in glassy liquid by echo-detected epr spectroscopy. *Applied Magnetic Resonance*, 15:237–246, 1998.

[45] Anatolii. A. Vereshchagin, Daniil A. Lukyanov, Ilia R. Kulikov, Naitik A. Panjwani, Elena A. Alekseeva, Jan Behrends, and Oleg V. Levin. The fast and the capacious: A [ni(salen)]-tempo redox-conducting polymer for organic batteries. *Batteries & Supercaps*, 4:336–346, 2020.

[46] Anatoliy A. Vereshchagin, Arseniy Y. Kalnin, Alexey I. Volkov, Daniil A. Lukyanov, and Oleg V. Levin. Key features of tempo-containing polymers for energy storage and catalytic systems. *Energies*, 15:1–50, 2022.

[47] Yuan Xie, Kai Zhang, Yusuke Yamauchi, Kenichi Oyaizu, and Zhongfan Jia. Nitroxide radical polymers for emerging plastic energy storage and organic electronics: Fundamentals, materials, and applications. *Materials Horizons*, 8:803–829, 2021.

[48] Chengjian Xu, Qiang Dai, Linda Gaines, Mingming Hu, Arnold Tukker, and Bernhard Steubing. Future material demand for automotive lithium-based batteries. *Communications Materials*, 1:1–10, 2020.

[49] Hyun Deog Yoo, Elena Markevich, Gregory Salitra, Daniel Sharon, and Doron Aurbach. On the challenge of developing advanced technologies for electrochemical energy storage and conversion. *Materials Today*, 17:110–121, 2014.

[50] E K Zavoisky. Paramagnetic relaxation of liquid solutions for perpendicular fields. *Zhur. Eksperiment. i Theoret. Fiz.*, 15:344–350, 1945.

[51] Clara Zens, Christian Friebe, Ulrich S. Schubert, Martin Richter, and Stephan Kupfer. Tailored charge transfer kinetics in precursors for organic radical batteries – a joint synthetic-theoretical approach. *ChemSusChem*, e202201679:1–14, 2022.

[52] Guangxu Zhang, Xuezhe Wei, Siqi Chen, Guangshuai Han, Jiangong Zhu, and Haifeng Dai. Investigation the degradation mechanisms of lithium-ion batteries under low-temperature high-rate cycling. *ACS Applied Energy Materials*, 5:6462–6471, 2022.

[53] Qingsong Zhang, Tiantian Liu, and Qiong Wang. Experimental study on the influence of different heating methods on thermal runaway of lithium-ion battery. *Journal of Energy Storage*, 42:1–9, 10 2021.